Automatic Segmentation of Brain Structures Using Geometric Moment Invariants and Artificial Neural Networks

Mostafa Jabarouti Moghaddam[1] and Hamid Soltanian-Zadeh[1,2]

[1] Control and Intelligent Processing Center of Excellence, Department of Electrical and Computer Engineering, University of Tehran, Tehran, Iran
[2] Image Analysis Laboratory, Department of Radiology, Henry Ford Hospital, Detroit, Michigan, USA
m.jabarouti@ece.ut.ac.ir, hszadeh@ut.ac.ir, hamids@rad.hfh.edu

Abstract. We propose an automatic method for the segmentation of the brain structures in three dimensional (3D) Magnetic Resonance Images (MRI). The proposed method consists of two stages. In the first stage, we represent the shape of the structure using Geometric Moment Invariants (GMIs) in 8 scales. For each scale, an Artificial Neural Network (ANN) is designed to approximate the signed distance function of a desired structure. The GMIs along with the voxel intensities and coordinates are used as the input features of the ANN and the signed distance function as its output. In the second stage, we combine the outputs of the ANNs of the first stage and design another ANN to classify the image voxels into two classes, inside or outside of the structure. We introduce a fast method for moment calculations. The proposed method is applied to the segmentation of caudate, putamen, and thalamus in MRI where it has outperformed other methods in the literature.

Keywords: Magnetic Resonance Images, Geometric Moments Invariants, Artificial Neural Network, automatic segmentation.

1 Introduction

Segmentation of the brain structures in Magnetic Resonance Images (MRI) is the first step in many medical image analysis applications and is useful for the diagnosis and evaluation of the neurological diseases such as autism, depression, fetal alcohol syndrome, Alzheimer's, and Parkinson's. Therefore, accurate, reliable, and automatic segmentation of the brain structures can improve diagnostic and treatment of the related neurological diseases. Manual segmentation by an expert is usually accurate but is impractical for large datasets because it is a tedious and time consuming process.

Until now, several methods have been developed for tissue segmentation and classification using MRI. These methods suffer from problems such as low contrast, discontinuous boundaries of the structures, ill-defined boundaries due to partial volume effect, intensity inhomogeneities [1], and low signal-to-noise ratio (SNR) [2]. On the

J.L. Prince, D.L. Pham, and K.J. Myers (Eds.): IPMI 2009, LNCS 5636, pp. 326–337, 2009.

other hand, different subjects with different ages and genders have structures with a variety of different shapes and specifications. To solve these problems, the proposed methods should benefit from prior knowledge of the structures. In this direction, several approaches have been developed using shapes of the structures [3,4] into the deformable model equations [5], regional information such as histogram [6], relationships among the neighboring structures [7,8], probabilistic atlas priors [9,10], boundary information [11,12], multiscale Bayesian framework [25], pattern recognition techniques such as Artificial Neural Network (ANN) as classifiers [13,14], Support Vector Machine (SVM) [15], and fuzzy sets with deformable models [16,17].

We focus on the methods that use the ANN as a classifier to segment the brain structures. An earlier method developed by Magnotta et al [13] used voxel intensity values of the neighboring voxels as the input feature. Their task was to classify the voxels into two classes – being inside or outside of the structure. They designed one ANN for each structure. The input features did not contain any shape representations. This causes the need for large training data sets. On the other hand, voxel intensity values can solve the segmentation problem for the high-resolution MRI they utilized. Recently, Powell et al [14] developed their previous algorithm [13] and added 9 voxel intensity values along the largest gradient, one probabilistic map value, and voxel intensity values along each of the three orthogonal values as the input features. They used high-resolution images the same as [13] for the segmentation of the brain structures. They used 15 images as the training data sets that were collected using two protocols: T1-weighted and T2-weighted.

In [18], we proposed the use of a new input feature – Geometric Moment Invariants (GMIs) [19] to improve the differentiation between the brain regions compared to the image intensity values. The GMIs characterize the underlying anatomical structures calculated for each voxel [19]. They are eleven moment invariants that are calculated from the first-order, second-order, and third-order 3D-regular moments. They are invariant to translation and rotation. For the first time, Shen et al [20] used the GMIs for elastic registration of MRI. They utilized them to reflect the underlying anatomy at different scales. They defined similarity measures instead of using a classifier to identify the brain structures. They optimized an objective function to maximize the image similarity.

In [18], we utilized an ANN for the segmentation of the putamen. The input features were the GMIs along the neighboring voxel intensity values. We calculated the GMIs for one scale. The output of the ANN was a single node that took two values (-1, 1) for indicating inside of the structure or its outside. However, one scale was not sufficient to distinguish all parts of the putamen.

In this research, we propose a two-stage method for the segmentation of the brain structures. In the first stage, we consider the shape of the structures using the GMIs in different scales along with the neighboring voxels intensity values as the input features and the signed distance function of the structure as the outputs of the ANNs. In each scale, an ANN is designed to approximate the signed distance function of the structure. In the second stage, we combine the outputs of the ANNs by another ANN to classify the voxels. By calculating the GMIs in different scales and using them as input features, we are able to produce excellent results using significantly smaller training data sets.

Our method has multiple advantages compared to the previous methods. First, it does not need to solve the optimization problem that can be very time consuming. The use of the ANNs decreases the processing time of the algorithm. Calculation of the GMIs in different scales is time consuming but we decreased this time by using a proposed fast moment calculation method and multi-threaded programming. Therefore, our proposed method is sufficiently fast its excellent performance.

This paper is organized as follows. The next section (Method Section) describes the first stage of the method for representing the shapes of the structures. Then, it describes the second stage of the method for classifying the voxels into two classes. Next, the Results Section presents the results of our algorithm for the segmentation of caudate, putamen, and thalamus. It also compares the proposed method with a number of previously published methods and illustrates its superiority. Finally, the Conclusion Section concludes the work and presents future directions.

2 Method

The proposed method has two stages. The shape of the structure is represented in the first stage and the desired structure is segmented in the second stage.

2.1 First Stage – Shape Representation

In the first stage, the GMIs are used with the voxel intensity values as the input features and the signed distance function of the desired structure as the output of an ANN. In this stage, there is one ANN for each scale of the GMIs. The GMIs are defined later in this section.

Pre-processing. The proposed method requires the datasets to be registered to a template. We register the datasets to the Montreal Neurological Institute (MNI) atlas using the FSL software [21].

The atlas-based method allows generation of a mask that has a high probability to include pixels of the desired structure in it. To create this mask for each structure, we sum all of the training datasets and smooth the results using a mean filter with a kernel size of 4 in 3D. The voxels which have positive values define the mask. We utilize 12 subjects of the IBSR datasets [22] for the training datasets.

ANN Architecture. The Multi Layer Perceptron (MLP) neural network is used to establish the relation between the input and output features. Several configurations for the MLP network are investigated. A set of multiple MLP networks are used finally as a setting with a good generalization. There are 33 neurons (the dimension of the input features) in the input layer, 17 neurons in the first hidden layer, 7 neurons in the second hidden layer, and a single neuron in the output (Fig. 1). The activation function used in the MLP network is the sigmoid function in all layers. The ANNs in this stage are used for function approximation.

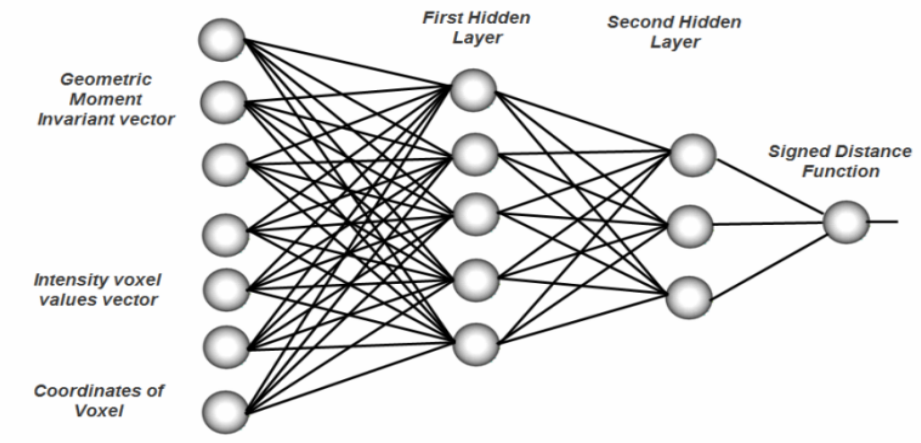

Fig. 1. ANN architecture of the first stage. Input features contain three components – GMIs, voxel intensity values, and coordinates of voxels. There are two hidden layers. There are 33 neurons in the input layer, 17 neurons in the first hidden layer, 7 neurons in the second hidden layer and a single neuron in the output. The output of the ANN is designed to approximate the singed distance function of the desired structure.

Input Features. Each input feature vector includes the neighbouring voxel intensity values, the GMIs, and the coordinates of the voxels. More formally, at voxel x, the input feature vector $a(x)$ is the concatenation of three row vectors, i.e., $a(x) = [a_1(x)\, a_2(x)\, a_3(x)]$ where $a_1(x)$ includes the voxel intensity values, $a_2(x)$ includes the coordinates of the voxel, and $a_3(x)$ includes the GMIs.

The vector $a_1(x)$ contains the neighbouring voxel intensity values of voxel x. We define $a_1(x)$ by considering the neighbouring voxels along the three orthogonal axes (± 3 voxels in each direction) in 3D. Therefore, the dimension of $a_1(x)$ **is** 19 including the intensity value of the voxel in the center (Fig 2.).

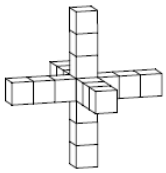

Fig. 2. Neighboring voxel intensity values that are considered for each voxel of the training datasets as a part of the input features

The vector $a_2(x)$ consists of the coordinates of the voxels in the Cartesian coordinate system. They help the ANN to find the relation between the voxels of the structure. The brain structures may have discontinuity in the image intensities inside the

structure and thus considering the coordinates of the voxels in the input features helps the ANN to fill in the discontinuities and generate continuous results.

The vector $a_3(x)$ contains the GMIs at voxel x. The GMIs include rich geometric properties that represent the underlying anatomical structures and thus help the ANN to distinguish between the voxels inside and outside of the desired structure. In [19], Lo et al explicitly defined 11 moment invariants consisting of the first, second, and third order 3D-regular moments. They introduced the notion of complex moments. Complex moments are defined as linear combinations of the moments with complex coefficients.

The GMIs are calculated as follows. Suppose the origin of the coordinate system is shifted to the voxel x. Then, the 3D-regular moments of order $(p+q+r)$ for the membership function $f_{tissue}(x_1, x_2, x_3) = \{image\}$ are defined by

$$M_{p,q,r} = \iiint_{(x_1)^2+(x_2)^2+(x_3)^2<R^2} x_1^p x_2^q x_3^r f_{tissue}(x_1, x_2, x_3) dx_1 dx_2 dx_3 \tag{1}$$

where R is the radius of the spherical neighbourhood around the origin. Due to the complexity of the formulas, we only present the second order moments below. Other formulas can be found in [19].

$$I_1 = M_{2,0,0} + M_{0,2,0} + M_{0,0,2} \tag{2}$$

$$I_2 = M_{2,0,0}M_{0,2,0} + M_{2,0,0}M_{0,0,2} + M_{0,2,0}M_{0,0,2} - M_{1,0,1}^2 - M_{1,1,0}^2 - M_{0,1,1}^2 \tag{3}$$

$$I_3 = M_{2,0,0}M_{0,2,0}M_{0,0,2} - M_{0,0,2}M_{1,1,0}^2 + 2M_{1,1,0}M_{1,0,1}M_{0,1,1} - M_{0,2,0}M_{1,0,1}^2 - M_{2,0,0}M_{0,1,1}^2 \tag{4}$$

In this research, 8 scales have been considered for R={2,3,4,5,6,8,10,12}. Although more scales can be considered, this will substantially increase the computation time. Each scale can detect some parts of the structure of interest. In this case, in each scale, we collect more information from the structure which is desirable.

Considering the above, the input feature vector is made of 33 features including 19 features for the voxel intensity values, 11 features for the GMIs, and 3 features for the coordinates of the voxel in the center of the neighbourhood.

Fast Moment Calculation. Calculation of the moment invariants is time-consuming. There are algorithms in the literature for reducing the computational complexity of the moment invariants [23,24]. However, they are appropriate for binary and 2D datasets. In our research, we use two tricks for fast moment calculation. First, we use the relation between successive voxels in the 3D datasets. Second, we use multithreading programming to reduce the processing time.

Usually, spheres with radius R are considered to calculate the regular moments using equation (1). This can be very time-consuming. The calculation complexity in this case is $O(R^3 \times M^3)$ where R is the radius used for the moment calculation and M is dimension of the volume over which to calculate the moments for each voxel inside it. We use the information of the previous voxel to calculate the moments. For voxel at position (x,y,z+1), we use the moment at position (x,y,z) with some consideration.

Instead of spheres, we use cubes for moment calculation. A cube can be divided into $2\times R+1$ planes along the z-axis. We define a buffer of size $2\times R+1$ and then we assign each entry as a weighted sum of each plane along the x and y coordinates. For moment calculation of voxels at position x, calculation of a weighted sum along the z-axis yields the 3D-regular moment for voxel at position (x,y,z). For the voxel at (x,y,z+1), we just update the buffer for the new plane when z increases by one. The entry of the buffer for the first plane of the previous voxel is removed. Therefore, for the moment calculation, we just need to update the weighted values along the z axis (Fig. 3). At the end of the line along the z axis, we increase the value of y and then update our buffer for the new position at (x,y+1,z). Hereby, all of the moments for the remaining voxels are calculated. In this case, the calculation complexity is $O(R^3+R\times M^3)$. This shows that our algorithm is much faster than the regular calculation of the moments.

Another trick that we utilize for fast computation of the moments is multithreading. For the calculation of the GMIs, we need 12 orders of the 3D-regular moments. For fast calculation of GMIs, we divide these 12 orders into four groups and calculate each group with one core of the CPU. We use a computer with a quad core CPU and then use a thread for each group. Therefore, the speed for moment calculation is four times faster. For a volume with a dimension of $182\times 218\times 182$, calculation of a moment with a radius of 4 takes about two minutes.

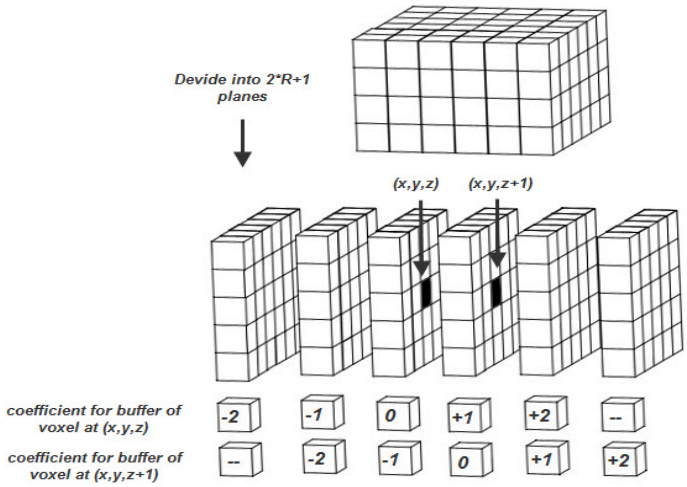

Fig. 3. Fast moment calculation method. In this figure, we demonstrate our method for the calculation of the moments with radius 2. For each voxel, we consider a cube with two voxels in each direction, therefore, the dimension of the cube is $5\times 5\times 5$. We show our method for two voxels at positions (x, y, z) and (x, y, z+1). At first, we construct the buffer for 5 planes of the first voxel. We assign each entry of the buffer as a weighted sum of each plane along the x- and y-coordinates. For moment calculation of the voxel at position (x, y, z), we multiply the coefficient vector (-2, -1, 0, 1, 2) by each entry of the buffer. For the next voxel at position (x, y, z+1), we calculate a weighted sum for a new plane and remove the first entry of the buffer and shift all entries by one to the right and then we calculate the new moment.

(a) (b)

Fig. 4. An example of the signed distance function for the putamen in an image of the training datasets. Fig. *(a)* shows a segmented putamen. Fig. *(b)* shows the signed distance function of Fig. *(a)*. Positive voxel values are normalized to [0 1] and negative voxel values are normalized to [-1 0].

Output Feature. Another trick used in our research for shape representation is to consider the output feature as a signed distance function of the structure of interest. The signed distance function is a subset of implicit functions in shape representations. It is defined to be positive in the interior, negative in the exterior, and zero on the boundary. Near the boundaries, the absolute values decrease and far from the boundaries they increase. In Fig. 4, an example is shown for the putamen.

The signed distance function improves the training of the ANNs. In this case, both of the input and output have the ability to represent the shape of the structure of interest.

Training ANN. The ANNs were trained using each voxel within the region of interest of the structure and the backpropagation algorithm. The training continued until the Mean Square Error (MSE) reached an asymptotic value. We did not expect the MSE to become zero because in each scale, the GMIs can detect some parts of the structure. The range of the MSE in the first stage is from 0.02 to 0.03. The training of an ANN takes about one day, thus, almost 9 days are needed for the training of the ANNs in both stages. Although this is a long time but it is performed only once.

2.2 Second Stage-Structure Identification

Each output of the first stage distinguishes different parts of the structure. The 8 outputs of the first stage are combined by an ANN in the second stage. This ANN works as a classifier not as a function approximator. The task of this stage is to classify the image voxels into two classes – being inside or outside of the structure. To remove outliers, the results of the ANNs of the first stage are smoothed using a mean filter with a kernel size of 3. Thus, the input features in this stage consist of the smooth versions of the 8 outputs of the first stage, 19 image intensity values of the neighbouring voxels along the three orthogonal axes, and the voxel coordinates in the Cartesian coordinate system. Consequently, the dimension of input feature vector is 30 here. The ANN setting used in this stage is the same as the ANN setting in the first stage. The lower the error in this stage, the better the results. The resulting network activation function is thresholded at 0 to define the structure of interest. The voxels that have an output value larger than 0 are considered as the

structure of interest and voxels that have an output smaller than 0 are considered as its outside.

Post-processing. There are small holes and outlier voxels that can be eliminated using morphological image processing methods. We utilize two morphological image processing methods: the image filling algorithm and the connected-component analysis. For filing the holes in the output of the ANN, we use the image filling algorithm and for eliminating the outlier voxels, we apply the connected-component analysis to find the largest connected component in 3D. This eliminates the outlier voxels.

Software. The training of the ANNs is implemented using the Matlab software ver. 2008a. The FSL software [21] is used for the registration algorithms. The calculation of the GMIs is performed by a program written in C programming language. The multi-threading is used to maximize the processing speed.

Datasets. We utilize 12 subjects of the IBSR datasets as the training datasets for all 6 structures. For the test datasets, we use three datasets. The first dataset includes the 6 remaining subjects of the IBSR and are used for the evaluation of the segmentation process on all of the 6 structures. The second datasets contains 8 subjects and is used for the evaluation of the segmentation process for the right and left putamen. The third dataset includes 6 subjects and is used for the evaluation of the segmentation process for the right and left caudate. All datasets include T1-weighted images. The second and third datasets are segmented by a local expert.

3 Results

Fig. 5 shows the outputs of the first stage for the putamen in the right hemisphere.

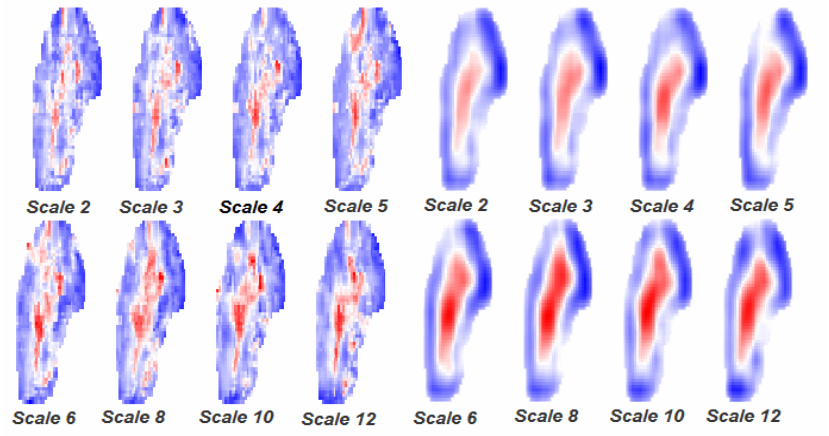

Fig. 5. Outputs of 8 ANNs of the first stage. Images on the left are outputs of ANNs in the first stage. Images on the right are the smoothed version of the images on the left.

(a) (b)

Fig. 6. The outputs of ANNs for three structures. *(a)* Manual segmentation by an expert. *(b)* Outputs of the second stage, i.e., the final segmentation by the proposed method.

Three-dimensional views of the putamen, caudate, and thalamus are shown in Figure 7.

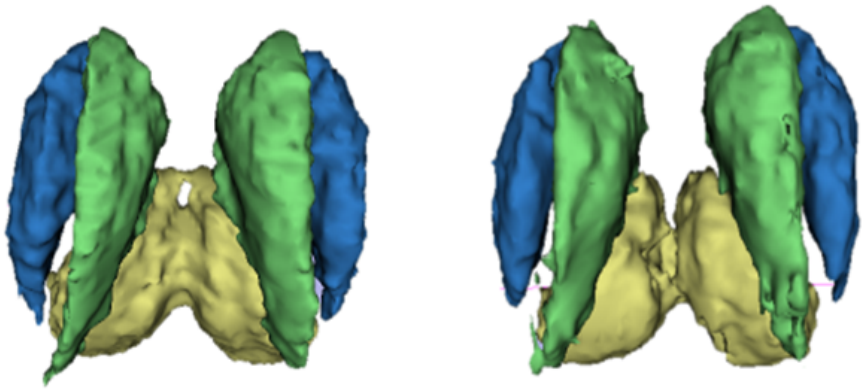

(a) (b)

Fig. 7. Three dimensional views of the outputs of three ANNs for three structures. *(a)* Manual segmentation by an expert. *(b)* Outputs of the proposed method. The caudate is shown in green, putamen is shown in blue, and thalamus is shown in yellow.

For quantitative comparisons, 3 measures are utilized. As a similarity index, the Dice Coefficient is calculated [17]. As distance indices, the H95 distance [25] and mean distance [17] are calculated. The results are presented in Table 1.

4 Conclusion

We presented a new method for the segmentation of the brain structures using the Geometric Moments Invariants and artificial neural networks. The GMIs along with

Table 1. Dice Coefficient, H95 Distance, and Mean Distance. Data in the form of Mean (standard deviation) is reported.

	Putamen	Caudate	Thalamus
Our Method			
Dice Coefficient	0.88 (0.01)	0.86 (0.02)	0.89 (0.01)
H95	1.92 (0.48)	2.40 (1.2)	2.21 (0.38)
Mean Distance	0.70 (0.13)	0.75 (0.2)	0.90 (0.15)
Previous Method [18]			
Dice Coefficient	0.85 (0.02)	---	---
Multi-scale Bayesian Method (Akselrod-Ballin et al [25])			
Dice Coefficient	0.79	0.80	0.84
H95	3.36	3.07	2.90
Mean Distance	1.60	1.44	1.44
Akhondi-Asl et al [7]			
Dice Coefficient	0.82	0.76	---
ISCA Method [15] (results reported in [25])			
Dice Coefficient	0.78	0.74	0.80
H95	3.89	4.46	3.41
Mean Distance	1.72	1.84	1.59
Powell et al [14]*			
Dice Coefficient	0.92 (0.02)	0.91 (0.02)	0.93 (0.01)

* They have used their own datasets. Our method and other methods use the IBSR datasets.

the voxel intensities and coordinates and the signed distance function were the inputs and outputs of the ANNs, respectively, for shape representation in the first stage. The smoothed outputs of the first stage were used along with the voxel intensities and coordinates as the inputs of another ANN in the second stage. The output of this ANN defined the voxels inside the structure of interest.

The quantitative comparisons shown in Table 1 illustrate the superiority of the proposed method to other methods in the literature. Our previous method had a Dice Coefficient of about 0.85. This result was obtained when only 6 IBSR datasets were used for the testing of the ANNs, the region of interest was about one half of the region of interest in the new method, and the threshold of the output of the ANN was experimental. Also, for each structure only one ANN was used and the GMIs were calculated only for one scale.

In comparing our results with the method proposed by Powell et al [14], note that their Dice Coefficients are higher than ours. However, they used two high resolution MR images acquired in their institution by T1-weighted and T2-wieghted protocols (not the IBSR datasets). The IBSR datasets contain T1-weighted images only and for a variety of subjects with different ages and genders. The ages of the subjects range from 7 to 71 years. Having access to a single modality (instead of dual modality) and large range for the subjects' ages make the segmentation task hard. In addition, they utilized larger datasets. Their method did not contain any shape representation methods. On the other hand, they used two other methods, template-based method and probability method for constructing their input features. They utilized the voxel intensity values along the largest gradient. Obviously, in low-resolution images with intensity inhomogeneity inside the structure, this feature may not work well.

For further evaluation of our method, we compared the results with those of other methods in the literature that used the IBSR datasets. In all of the cases, our method is at least 5% superior to the others in terms of the Dice coefficient. Moreover, our H95 distances and mean distances are smaller than those of the other algorithms. Due to the nature of the neural network-based methods, we have more outlier voxels than the other methods. In spite of this limitation, our method is superior to the others. Sample results are shown in Figures 6-7 for visual inspection.

Akhondi-Asl et al [7] utilized 10 subjects for the training and 8 remaining subjects of the IBSR for the testing. Akselrod-ballin et al [25] incorporated the prior knowledge information into a multi-scale framework. In that work, the probability information constructed with the IBSR datasets was based on an atlas prior and on a likelihood function. 5 subjects of the IBSR datasets were used for constructing the atlas prior and 17 subjects were used for constructing the likelihood function. Their algorithm was tested on the 18 subjects of the IBSR. We tested our algorithm on 14 subjects for the putamen, 12 subjects for the caudate and 6 subjects for the thalamus.

Overall, we established a new framework for the segmentation of the brain structures in MRI. The proposed method can be extended to improve its performance. Alternative input features, a different number of scales for the first stage, and other design methods for the second stage can be investigated. For example, the level set method can be used in the second stage. Using the signed distance function available as the output of the first stage, the level set equations become simple. A framework can be established for combining all of the ANNs to develop a single network for the segmentation process. For the input feature, the use of the probability information such as prior atlas [14,25] and the use of the logarithm of the odds ratio, which encodes shapes of multiple anatomical structures with capturing some information concerning uncertainty [26], can be useful. Last but not least, the proposed method can be applied to the segmentation of other brain structures in MRI and other organs in other medical images.

References

1. Macovski, A.: Noise in MRI. Magnetic Resonance in Medicine 36(3), 494–497 (1996)
2. Simmons, A., Tofts, P.S., Baker, G.J., Arridge, S.R.: Sources of Intensity Nonuniformity in Spin Echo Images at 1.5T. Magnetic Resonance in Medicine 32(1), 121–128 (1994)
3. Leventon, M.E., Grimson, W.E.L., Faugeras, O.: Statistical Shape Influence in Geodesic Active Contours. In: IEEE International Conference on Computer Vision and Pattern Recognition, vol. 1, pp. 1316–1323 (2000)
4. Jehan-Besson, S., Herbulot, A., Barlaud, M., Aubert, G.: Shape Gradient for image and Video Segmentation. Mathematical Models in Computer Vision, The Handbook (2005)
5. Kass, M., Witkin, A., Terzopoulos, D.: Snakes: Active Contour Models. In: First International Conference on Computer Vision, pp. 259–268 (1987)
6. Woolrich, M.W., Behrens, T.E.: Variational Bayes Inference of Spatial Mixture Models for Segmentation. IEEE Transaction on Medical Imaging 25(10), 1380–1391 (2006)
7. Akhondi-Asl, A.R., Soltanian-Zadeh, H.: Constrained Optimization of Nonparametric entropy-based Segmentation of brain Structures. In: IEEE ISBI 2008, pp. 4–44 (2008)
8. Tsai, A., Wells, W., Tempany, C., Grimson, E., Willsky, A.: Mutual Information in Coupled Multi-Shape Model for medical Image Segmentation. Medical Image Analysis 8(4), 429–445 (2004)

9. Gouttard, S., Styner, S., Joshi, S., Smith, R.G., Cody, H., Gerig, G.: Subcortical Structure Segmentation using Probabilistic Atlas priors. In: Proc. SPIE, vol. 6512 (2007)
10. Liu, J., Chelberg, D., Smith, C., Chebrolu, H.: Automatic Subcortical Structure Segmentation Using probabilistic Atlas. In: Bebis, G., Boyle, R., Parvin, B., Koracin, D., Paragios, N., Tanveer, S.-M., Ju, T., Liu, Z., Coquillart, S., Cruz-Neira, C., Müller, T., Malzbender, T. (eds.) ISVC 2007, Part I. LNCS, vol. 4841, pp. 170–178. Springer, Heidelberg (2007)
11. Angelini, E.D., Jin, Y., Laine, A.F.: State-of-the-Art of levelset Methods in Segmentation and Registration of Medical Imaging Modalities. In: The handbook of Medical Image Analysis. Registration Models, vol. 3. Kluwer Academic/Plenum publishers, New York (2005)
12. Jacob, M., Blu, T., Unser, M.: Efficient energies and algorithms for parametric snakes. IEEE Transactions on Image Processing 13(9), 1231–1244 (2004)
13. Magnotta, V.A., Heckel, D., Andreasen, N.C., Cizadlo, T., Corson, P.W., Ehrhardt, J.C., Yuh, W.T.: Measurement of brain Structures with Artificial neural Network: two and three-dimensional applications. Radiology 211(3), 781–790 (1999)
14. Powell, S., Magnotta, V.A., Johnson, H., Jammalamadaka, V.K., Prerson, R., Anderasen, N.C.: Registration and Machine Learning-based Automated Segmentation of Subcortical and Cerebellar brain Structures. NeuroImage 39, 238–247 (2008)
15. Akselrod-Ballin, A., Galun, M., Gomori, M.J., Basri, R., Brandt, A.: Atlas Guided Identification of Brain Structures by Combining 3D Segmentation and SVM Classification. In: Larsen, R., Nielsen, M., Sporring, J. (eds.) MICCAI 2006. LNCS, vol. 4191, pp. 209–216. Springer, Heidelberg (2006)
16. Amini, L., Soltanian-Zadeh, H., Lucas, C., Gity, M.: Automatic Segmentation of Thalamus from brain MRI Integrating fuzzy clustering and dynamic contours. IEEE Transactions on Biomedical Engineering 51, 800–811 (2004)
17. Ciofolo, C., Barillot, C.: Brain Segmentation with Competitive level sets and fuzzy control. In: Christensen, G.E., Sonka, M. (eds.) IPMI 2005. LNCS, vol. 3565, pp. 333–344. Springer, Heidelberg (2005)
18. Jabarouti Moghaddam, M., Rahmani, R., Soltanian-Zadeh, H.: Automatic Segmentation of Putamen using Geometric Moment Invariants. In: The 15th Iranian Conference on Biomedical Engineering, Mashad, Iran (2009)
19. Lo, C.H., Don, H.S.: 3-D Moment Forms: Their Construction and Application to Object Identification and Positioning. IEEE Trans. on Pattern Analysis and Machine Intelligence 11(10), 1053–1064 (1989)
20. Shen, D., Davatzikos, D.: HAMMER: Hierarchical Attribute Matching Mechanism for elastic Registration. IEEE Trans. Med. 21(11), 1421–1439 (2002)
21. Jenkinson, M., Bannister, P., Brady, M., Smith, S.: Improved Methods for the Registration and Motion Correction of Brain Images. NeuroImage 17(2), 825–841 (2002)
22. The Internet Brain Segmentation Repository, `http://www.cma.mgh.harvard.edu/ibsr`
23. Shen, B.C., Shen, J.: Fast Computation of Moment Invariants. Pattern Recognition 24, 801–806 (1991)
24. Zakaria, M.F., Vroomen, L.J., Zsomhar-Murray, P.J.A., Kessel, M.H.M.V.: Fast Algorithm for Computation of Moment Invariants. Pattern Recognition 20, 634–643 (1987)
25. Akselrod-Ballin, A., Galun, M., Gomori, M.J., Basri, R., Brandt, A.: Prior Knowledge Driven Multiscale Segmentation of Brain MRI. In: Ayache, N., Ourselin, S., Maeder, A. (eds.) MICCAI 2007, Part II. LNCS, vol. 4792, pp. 118–126. Springer, Heidelberg (2007)
26. Pohl, K.M., Fisher, J., Bouix, S., Shenton, M., McCarley, R.W., Grimson, W.E.L., Kikinis, R., Wells, W.M.: Using the Logarithm of Odds to Define a Vector Space. Medical Image Analysis 11, 465–477 (2007)